

Affine-invariant curvature estimators for implicit surfaces

MARIA ANDRADE AND THOMAS LEWINER

Department of Mathematics — Pontifícia Universidade Católica — Rio de Janeiro — Brazil
www.matmidia.mat.puc-rio.br/{maria,tomlew}.

Abstract. Affine Differential Geometry provides a set of measures invariant under a larger set of transformations compared to rigid motions. This leads to several applications using robust shape descriptors. Although affine invariant operations are already used for surfaces, they do not intend to approximate the definitions of Affine Differential Geometry, which are the basis for further differential invariants. In this work we propose estimators for the local affine structure of an implicit surface, i.e. the affine metric, the co-normal and normal vectors, and the affine Gaussian and mean curvatures. The direct derivation of the formulae from the implicit function theorem lead to very intensive computations and numerical instabilities. This work further proposes a geometrical reduction allowing a much simpler and more stable formulae, and compares the results by incorporating the proposed estimators in Marching Cubes based algorithms.

Keywords: *Affine curvature. Implicit surface. Isosurface. Affine invariants. Gaussian curvature. Mean curvature.*

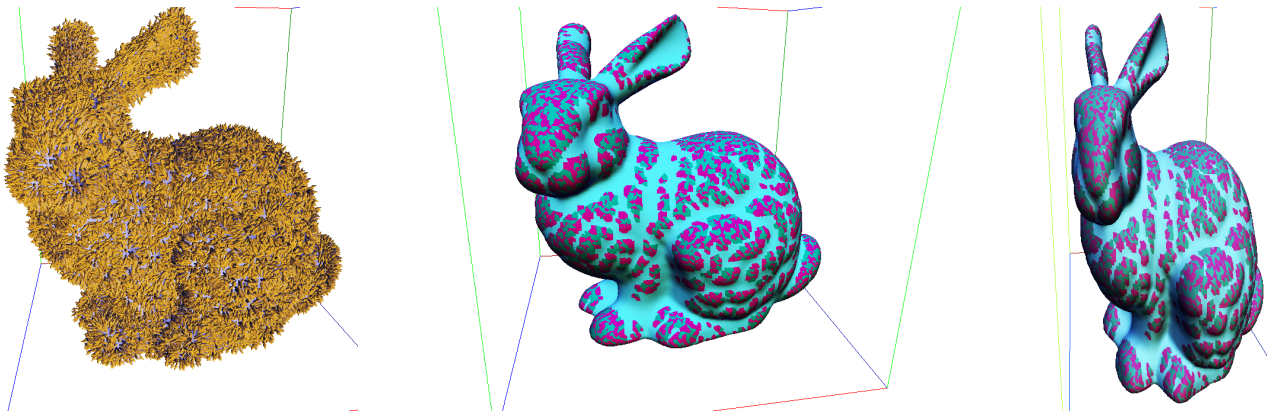


Figure 1: On a complex isosurface, here from a discretization of the distance to the Stanford Bunny on a 129^3 grid, the estimated Gaussian affine curvatures correspond.

1 Introduction

Implicit representation of geometric models are widely used, in particular for their design versatility, such as the efficient representation for deformation, Boolean operations and offsets [7]. The computation of the topological and geometrical structure from such representations may be delicate, although it is well known for parametric representations [5]. In particular, the curvature formulae for implicit surfaces were not gathered until recently [12], and their topological structure is tricky to compute [22]. In this paper we provide formulae with geometrical reductions to compute the affine structure of implicit surfaces and numerical tools to incorporate them into *Marching Cubes* based algorithms [16].

Affine invariant measures have received a lot of attention recently in the computer vision community for improving matching and registration [18, 19, 29]. Indeed, curves on an object seen from two different views have different Euclidean measures, i.e. distances or curvatures [17]. However, if the curve is contained in a plane parallel to the projection plane, the affine measures would correspond across photos. For three-dimensional data, the quantification of shape similarities have already a large number of applications in matching and recognition [1, 10, 26] and reconstruction [11]. Although some objects are clearly similar they do not match locally under rigid motion (see Figure 1). A better similarity measure for such objects may be obtained using a

larger set of transformations, requiring more sophisticated measures. From this point of view, the simplest geometry beyond the Euclidean one is the affine geometry, which defines measures that are invariant under affine transformation, i.e. including non-uniform scaling and shearing. This paper introduces estimators of such measures for surfaces represented implicitly.

Related work Planar affine geometry is commonly used in image processing and computer vision, from affine curve motion [28, 9] to affine invariant descriptors [18]. Those works are motivated by the geometrical description of viewpoint changes in photographic projections, which are well approximated by affine transformations [17]. In particular, Mikolajczyk *et al.* [18] provide a survey of local shape descriptor, with emphasis on affine invariant ones [18, 19]. For planar curves described explicitly, Craizer *et al.* [6] propose a local affine-invariant construction of parabolic polygons, from which they deduce the affine length, normal and curvature of the discrete curve. Zuliane *et al.* [29] propose an global affine-invariant descriptor based on Helmholtz's equation for vibrating membrane with a matching application. In this work we propose local affine normals and curvatures estimators for implicit surfaces.

For three dimensional shapes, affine invariant descriptors have been studied since 1990's. Already Arbter *et al.* [1] derive global affine invariant descriptors for parametric models through normalization of the Fourier transform. Mortara and Patané [21] derive affine invariant skeleton for 3d shapes using partial barycenters to embed the Reeb graph of the shape. Betelu *et al.* [2] define 3d affine invariant distances to also derive a skeleton by erosion. Rothganger *et al.* [27] propose to use affine-invariant neighborhoods in 3d shapes to derive affine descriptors from local parameterization. Raviv *et al.* [25] show how affine invariant descriptors on 3d meshes improve several practical applications such as shape characterization, triangulation, non-rigid shape matching and intrinsic symmetry detection. In particular, they extend the 3d shape descriptors with approximation of geodesics for the equi-affine metric [13]. In this work, we propose to approximate affine curvatures, which are the basis for further local differential affine invariants. Such estimators are derived in an implicit setting, following the approach from Goldman [12] and references therein.

Contributions In this paper we describe the affine structure of a surface, i.e. affine co-normal, normal vectors, and affine curvatures, for the case where S is a graph, and derive the formulae for the implicit case (see section 2). The direct computation of those leads to more than 23,000 flops per point of estimation, which leads to large numerical instabilities. Therefore, we propose a mapping from the local geometry via an affine transformation to get a simpler case with gradient vector $\nabla f = [0, 0, 1]$ and principal curvatures aligned with the global frame. In this case, simplified formulae can be applied, reducing to approximately 1,500 flops per point (see section 3). We describe how to incorporate such estimators in Marching Cubes [16] based algorithm (see section 4) and perform some numerical experiments with our estimators (see section 5).

Throughout this work, we study invariant structures under the equiaffine group of transformations, i.e. transformations of the form $p \mapsto Ap + t$ where A is a 3×3 matrix of determinant 1 and t is a vector in \mathbb{R}^3 . The translation part t has only trivial impact on the geometric structures and will be omitted hereafter. We use the term affine instead of equiaffine to ease the reading. We use the notation f_x for the partial derivative of f along the x direction. Finally, in the theoretical development we will consider only functions of class C^4 at regular points.

2 Affine structures and their formulae in the graph and implicit cases

In this section we will give some definitions of the main affine structures: the co-normal and normal vectors, and the Gaussian and mean curvatures. We will give the formulae for surfaces described as a graph, and deduce those for the implicit case using the implicit function theorem, as Goldman did for the Euclidean case. In essence, for quadrics, the affine normal points towards the center of the quadric. For general surfaces, the centers of mass of successive cuts parallel to the tangent plane near a point p define a curve, whose tangent direction at p is given by the surface's affine normal at p . Then, affine curvature is given by the variation of the affine normal. A more complete exposition of affine structures can be found in the books of Buchin [3] or Nomizu [23].

(a) Derivatives of an implicit surface

We consider here the affine structure of a surface described implicitly $S = \{ (x, y, z) \in \mathbb{R}^3, f(x, y, z) = 0 \}$, where f is at least of class C^4 . Given a point $p \in S$ that is regular, i.e. $\nabla f(p) = [f_x, f_y, f_z] \neq 0$, we assume, without loss of generality that $f_z(p) \neq 0$. The implicit function theorem ensures the existence of a function $g : U \subset \mathbb{R}^2 \rightarrow \mathbb{R}$ such that the equation $z = g(x, y)$ describes the surface S in a neighborhood of p . Thus S can be parameterized around p as a graph $G = \{ \mathcal{G}(x, y) = (x, y, g(x, y)), (x, y) \in U \}$ on an open set $U \subset \mathbb{R}^2$. Although g is hard to find in general, the derivatives g at image point p are easily expressed from the derivatives of f :

$$\text{at } p = [x, y, g(x, y)] : \quad g_x(x, y) = -\frac{f_x(p)}{f_z(p)} \quad \text{and} \quad g_y(x, y) = -\frac{f_y(p)}{f_z(p)} . \quad (1)$$

Further derivatives of g can be obtained from those expressions using the chain rule from $p = [x, y, g(x, y)]$ [12].

Note that the formulas derived from the theorem may lead to numerical instabilities when $|f_z(p)|$ has a small value.

(b) Tangent plane and affine metric

The *tangent vectors*, combinations of $\mathcal{G}_x = [1, 0, g_x]$ and $\mathcal{G}_y = [0, 1, g_y]$, are naturally contravariant under any matrix transformation A , in particular equiaffine ones: if \mathbf{t} is tangent to S at point p , then $A\mathbf{t}$ is tangent to the image of S by A at point Ap (a consequence of the chain rule).

The usual affine metric on this tangent plane is the *Berwald-Blaschke* metric, which corresponds to the elementary volume of a curve frame on the surface. It can be expressed by the bilinear form $d^{-1/4} \begin{bmatrix} L & M \\ M & N \end{bmatrix}$ with:

$$\begin{aligned} L &= \det | \mathcal{G}_x, \mathcal{G}_y, \mathcal{G}_{xx} | = g_{xx}(x, y), & M &= \det | \mathcal{G}_x, \mathcal{G}_y, \mathcal{G}_{xy} | = g_{xy}(x, y), \\ N &= \det | \mathcal{G}_x, \mathcal{G}_y, \mathcal{G}_{yy} | = g_{yy}(x, y), & d &= LN - M^2 = g_{xx}g_{yy} - g_{xy}^2. \end{aligned}$$

Throughout the theoretical developments, we suppose that the Berwald-Blaschke metric is non-degenerate: $d \neq 0$. Geometrically $d > 0$ means that the Euclidean Gaussian curvature does not vanish, i.e. the surface is strongly convex. The local affine surface area form is then given by $|d|^{1/4} \cdot \mathbf{d}x \wedge \mathbf{d}y$.

The implicit formulae for the metric can be derived using Equation (1):

$$\begin{aligned} g_{xx} &= -\frac{f_{xx}}{f_z} + \frac{2f_{xz}f_x}{f_z^2} - \frac{f_{zz}f_x^2}{f_z^3}, \\ g_{xy} &= -\frac{f_{xy}}{f_z} + \frac{f_{yz}f_x + f_yf_{xz}}{f_z^2} - \frac{f_yf_{zz}f_x}{f_z^3} \\ g_{yy} &= -\frac{f_{yy}}{f_z} + \frac{2f_{yz}f_y}{f_z^2} - \frac{f_{zz}f_y^2}{f_z^3}. \end{aligned}$$

In particular:

$$\begin{aligned} d &= \frac{1}{f_z^4} \cdot \left(\begin{aligned} &(f_{yy}f_{zz} - f_{yz}^2)f_x^2 + 2(f_{xz}f_{xy} - f_{xx}f_{yz})f_yf_z + \\ &(f_{zz}f_{xx} - f_{xz}^2)f_y^2 + 2(f_{xy}f_{yz} - f_{yy}f_{xz})f_zf_x + \\ &(f_{xx}f_{yy} - f_{xy}^2)f_z^2 + 2(f_{yz}f_{xz} - f_{zz}f_{xy})f_xf_y \end{aligned} \right). \end{aligned} \quad (2)$$

(c) Affine co-normal

Orthonormality relationships are not preserved under an affine transformation A , therefore the Euclidean normal \mathbf{N}_e is not an affine covariant vector. However, the direction of the Euclidean normal is covariant (if $\langle \mathbf{N}_e, \mathcal{G}_x \rangle = 0$, then $\langle A^{-T}\mathbf{N}_e, A\mathcal{G}_x \rangle = 0$, and similarly for \mathcal{G}_y). Therefore, a covariant affine normal, called the *affine co-normal* ν , can thus be obtained by scaling the Euclidean normal vector [4] (see Figure 2):

$$\nu = |K_e|^{-1/4} \mathbf{N}_e = |g_{xx}g_{yy} - g_{xy}^2|^{-1/4} [-g_x, -g_y, 1], \quad (3)$$

where K_e is the Euclidean Gaussian curvature: $K_e = (1 + g_y^2 + g_x^2)^{-2}(g_{xx}g_{yy} - g_{xy}^2)$. This affine co-normal then satisfies $\langle \nu, \mathcal{G}_x \rangle = \langle \nu, \mathcal{G}_y \rangle = 0$ and the affine metric satisfies $d^{1/4} = \pm \det | \nu, \nu_x, \nu_y |$.

The implicit formulae for the co-normal can be derived from Equation (3):

$$\nu = \frac{1}{f_z d^{1/4}} [f_x, f_y, f_z].$$

The implicit formulae for the affine structures described in the following subsections can be similarly derived. The next session will describe formulae for a generic case, which are more numerically stable.

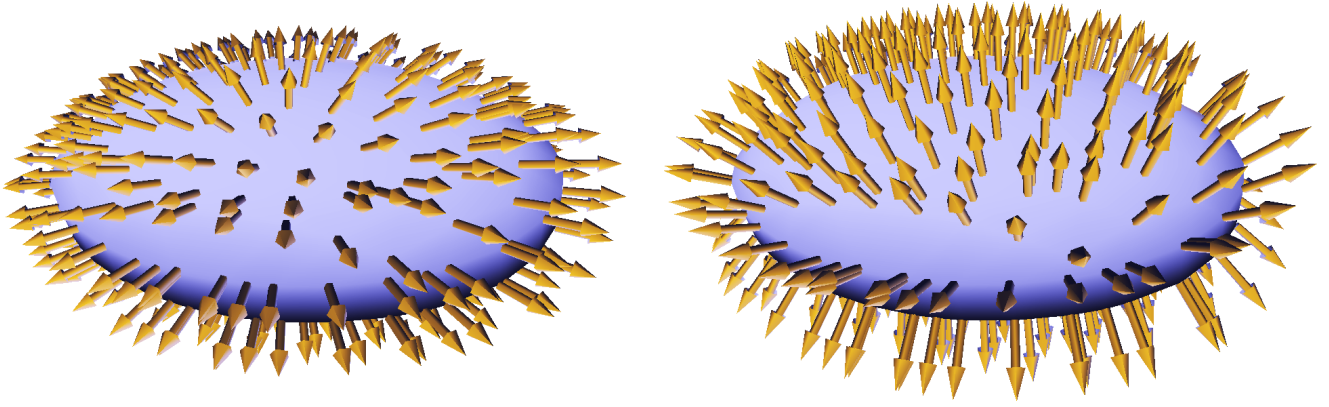


Figure 2: Affine co-normal ν (left) and normal ξ (right) directions on an ellipsoid: the affine co-normal is co-linear with the Euclidean one, while the affine normal points towards the center of the ellipse, emphasizing that an ellipsoid is the affine image of a sphere.

(d) Affine normal

Since the affine co-normal is not in general a unitary vector, it is not orthogonal to its derivatives ν_x, ν_y . But since $\det |\nu, \nu_x, \nu_y| = \pm d^{1/4} \neq 0$, those derivatives define a proper plane not orthogonal to ν . A contravariant affine vector can then be obtained by looking at a vector orthogonal to that plane and would be the affine equivalent to the Euclidean normal (see Figure 2). More precisely, the *affine normal* vector ξ is defined locally by the relationship:

$$\langle \nu, \xi \rangle = 1, \quad \langle \xi, \nu_x \rangle = \langle \xi, \nu_y \rangle = 0.$$

The affine normal then satisfies: $\langle \nu, \xi_x \rangle = \langle \nu, \xi_y \rangle = 0$ and $\det |\mathcal{G}_x, \mathcal{G}_y, \xi| = \pm d^{1/4}$. This last relation shows that a local basis for the embedding space \mathbb{R}^3 at a point p of the surface can be obtained by $\{\mathcal{G}_x, \mathcal{G}_y, \xi\}$. This allows to define affine structures from Cartan's moving frames theory [23].

Denote by $\xi = [\xi_1, \xi_2, \xi_3]$ the affine normal vector, we know that $\langle \xi, \nu \rangle = 1, \langle \nu, \xi_x \rangle = \langle \nu, \xi_y \rangle = 0$. Thus $\xi = \lambda (\nu_x \times \nu_y)$, with $\lambda = \det |\nu, \nu_x, \nu_y|^{-1} = d^{-1/4}$.

We can deduce the explicit formulas for the coordinates of ξ :

$$\begin{aligned} \xi_1 &= \frac{1}{4} d^{-7/4} (g_{xx}g_{xy}g_{yyy} - g_{xx}g_{yy}g_{xxy} - g_{yy}^2g_{xxx} - 2g_{xy}^2g_{xyy} + 3g_{yy}g_{xy}g_{xxy}), \\ \xi_2 &= \frac{1}{4} d^{-7/4} (g_{yy}g_{xy}g_{xxx} - g_{xx}g_{yy}g_{xxy} - g_{xx}^2g_{yyy} - 2g_{xy}^2g_{xxy} + 3g_{xx}g_{xy}g_{xyy}), \\ \xi_3 &= \frac{1}{4} d^{-7/4} (4g_{xy}^4 + 4g_{xx}^2g_{yy}^2 - 8g_{xx}g_{yy}g_{xy}^2 + 3g_xg_{yy}g_{xy}g_{xxy} + 3g_yg_{xx}g_{xy}g_{xyy} \\ &\quad - g_xg_{yy}^2g_{xxx} - g_yg_{xx}^2g_{yyy} - 2g_xg_{xy}^2g_{xyy} - 2g_yg_{x,y}^2g_{xxy} \\ &\quad - g_xg_{xx}g_{yy}g_{xyy} - g_yg_{xx}g_{yy}g_{xxy} + g_xg_{xx}g_{xy}g_{yyy} + g_yg_{yy}g_{xy}g_{xxx}). \end{aligned}$$

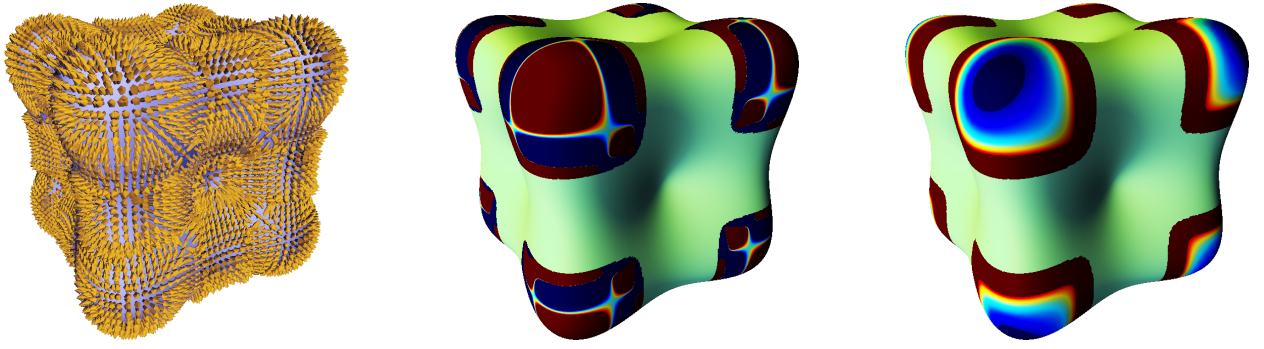


Figure 3: Affine structure of a blobby surface $(3x)^4 + (3y)^4 + (3z)^4 - 45x^2 - 45y^2 - 45z^2 + 6 = 0$: (from left to right) normal direction ξ , Gaussian \mathcal{K} and mean \mathcal{H} curvatures, colored from red to blue, the central green part corresponding to a degenerate metric.

(e) Affine curvatures

As in Euclidean geometry, the curvature describes the variations of the normal (see Figure 3). Since $\langle \nu, \xi_x \rangle = \langle \nu, \xi_y \rangle = 0$, the derivatives ξ_x, ξ_y of the affine normal are orthogonal to ν , which is parallel to \mathbf{N}_e . Therefore, ξ_x, ξ_y are tangent to the surface:

$$\xi_x = -b_{11} \mathcal{G}_x - b_{12} \mathcal{G}_y, \quad \xi_y = -b_{21} \mathcal{G}_x - b_{22} \mathcal{G}_y.$$

Consequently:

$$\begin{aligned} b_{11} &= -d^{-1/4} \cdot \det | \xi_x, \mathcal{G}_y, \xi |, & b_{12} &= -d^{-1/4} \cdot \det | \mathcal{G}_x, \xi_x, \xi |, \\ b_{21} &= -d^{-1/4} \cdot \det | \xi_y, \mathcal{G}_y, \xi |, & b_{22} &= -d^{-1/4} \cdot \det | \mathcal{G}_x, \xi_y, \xi |. \end{aligned}$$

The coefficients b_{ij} form a matrix $B = [b_{ij}]_{1 \leq i, j \leq 2}$, whose determinant and trace are respectively the Gaussian and mean affine curvatures: $\mathcal{K} = \det B$, $\mathcal{H} = \frac{1}{2} \text{tr } B$.

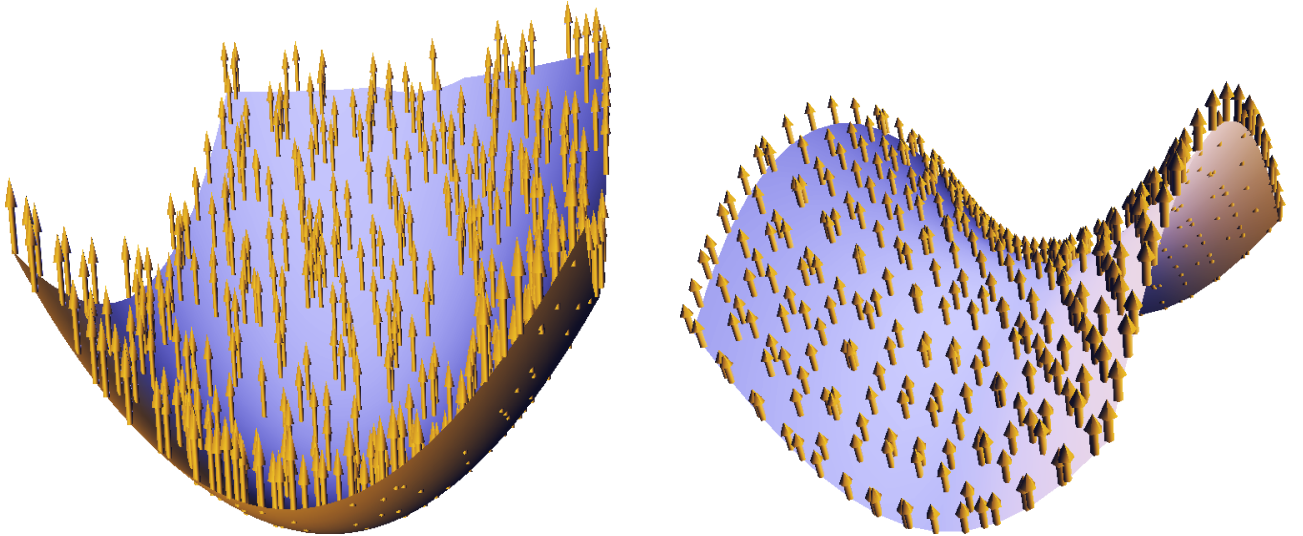


Figure 4: Elliptic and hyperbolic paraboloids have a constant affine normal ξ . They play the role of the Euclidean plane in affine geometry.

(f) Fundamental examples

The most basic shapes of Euclidean geometry are the plane, with constant normal and thus zero curvature, and the sphere, with constant curvature. In affine geometry, the equivalent shapes are the paraboloids, with constant affine normal (see Figure 4), and the ellipsoid and hyperboloids of one and two sheets, with constant curvatures, respectively. Their affine structures are collected below.

	Elliptic Paraboloid	Hyperbolic Paraboloid	Sphere
f	$z - \frac{1}{2}(x^2 + y^2)$	$z - \frac{1}{2}(x^2 - y^2)$	$x^2 + y^2 + z^2 - r^2$
\mathbf{N}_e	$\frac{1}{\sqrt{1+x^2+y^2}} \cdot [-x, -y, 1]$	$\frac{1}{\sqrt{1+x^2+y^2}} \cdot [-x, y, 1]$	$\frac{1}{r} \cdot [x, y, z]$
K_e	$(1 + x^2 + y^2)^{-2}$	$-(1 + x^2 + y^2)^{-2}$	r^{-2}
\mathbf{d}	1	-1	$r^2 z^{-4}$
ν	$[-x, -y, 1]$	$[-x, y, 1]$	$r^{-1/2} [x, y, z]$
ξ	$[0, 0, 1]$	$[0, 0, 1]$	$r^{-3/2} [x, y, z]$
\mathcal{K}	0	0	r^{-3}
\mathcal{H}	0	0	$-2r^{-3/2}$

3 Geometric reductions and simplified formulae

The formulae for the affine structures derived in the previous section are already extensive for the case of a graph $G = \{(x, y, g(x, y))\}$, and increase in size dramatically when using the implicit function theorem to express those affine structures directly in term of the implicit function f . This leads to significant numerical instability during the computation, and harms the affine invariance of the calculated quantities (see Figure 5).

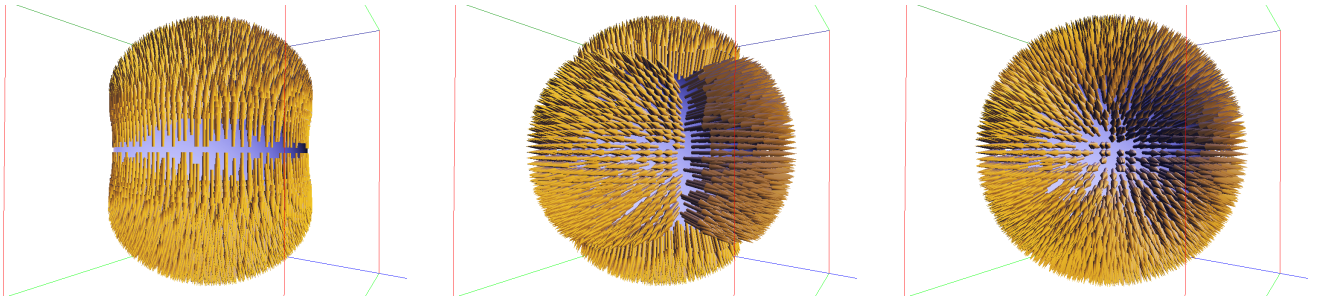


Figure 5: Affine normal ξ computed always using z in the implicit derivation of Equation (1) (left), the axis mostly aligned with the gradient (middle), or our geometric reduction (right).

However, we know how each affine quantity varies under an affine transformation: the metric and the affine curvatures are invariant, the co-normal is covariant and the normal is contravariant. Here we define an affine transformation A that simplifies the above formulae and improve (or isolate) numerical instability. This section will first introduce this transformation, derive the formulae for the affine structure after the simplification, and finally show how to compute the affine structure for a general implicit surface using this simplification.

(a) Simplifying transformation

Since all the implicit formulae are derived from the implicit function theorem (Equation (1)), most of the terms may be simplified if we can set the gradient of f to a constant vector, e.g. $[0, 0, 1]$, after an affine transformation A . Moreover, aligning the Euclidean principal curvature directions with the x -axis and y -axis further reduces the size of our formulae.

More precisely, we look for an (equi-)affine transformation A (neglecting the a translation part which has no effect on the derivatives) as the composition of a rotation R_1 and a scaling S that maps the gradient to a vertical direction with unit norm, and a rotation R_2 in the xy -plane to align the Euclidean principal curvatures (see Figure 6). The effect of this transformation on the derivatives is described in the following proposition and the construction of A is detailed in its proof.

Proposition 1 *At each regular point p of the implicit surface $\{p \in \mathbb{R}^3, f(p) = 0\}$, there exists an equiaffine transformation A such that, at point $\tilde{p} = A(p)$ of the transformed implicit surface $\{\tilde{p} \in \mathbb{R}^3, \tilde{f}(\tilde{p}) = f(A^{-1}(\tilde{p})) = 0\}$:*

- the gradient is the unit vertical vector: $\nabla \tilde{f}(\tilde{p}) = [0, 0, 1]$.
- the crossed derivative \tilde{f}_{xy} vanishes: $\tilde{f}_{xy}(\tilde{p}) = 0$.

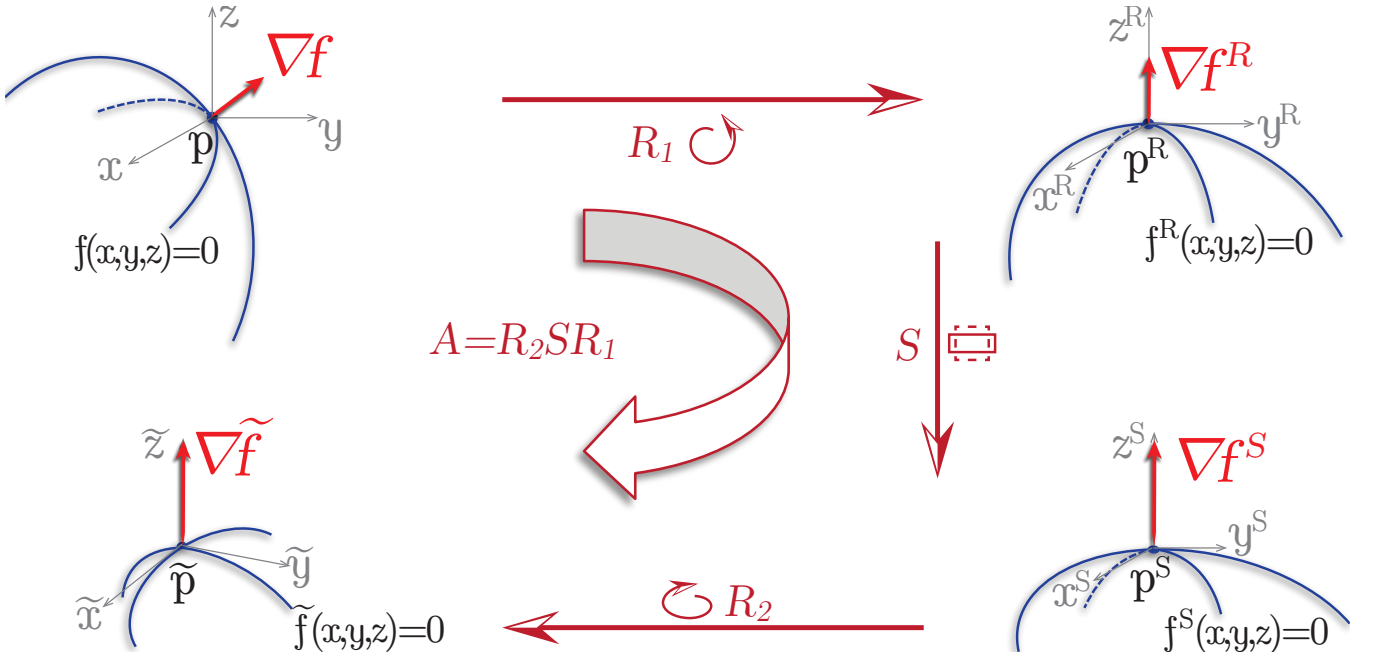


Figure 6: The construction of the transformation A .

Proof: First observe that $\nabla \tilde{f}(\tilde{p}) = \nabla f(p) \cdot A^{-1}$ (writing the gradient in line). We deduce the transformations for the first item with simple descriptive geometry: We decompose the equiaffine transformation as $A = R_2 S R_1$ (see Figure 6), where R_1 is a rotation in \mathbb{R}^3 , S is a non-uniform scaling along z and the xy -plane; and R_2 is a rotation in the xy -plane.

Rotation R_1 is a rotation mapping $\nabla f(p)$ to the vertical vector $[0, 0, \|\nabla f(p)\|]$. We denote by f^R the transformed implicit function: $f^R(p) = f(R_1^{-1}(p))$. We check the gradient vector of f^R : $[\nabla f^R]^T = R_1^{-T} [\nabla f]^T = R_1 [\nabla f]^T = [0, 0, \|\nabla f(p)\|]^T$.

Then, we scale the obtained gradient. However, to obtain an equiaffine transformation, we must compensate the scaling along z on the plane x, y . We thus define S as the diagonal matrix $S = \text{diag}(\eta^{-\frac{1}{2}}, \eta^{-\frac{1}{2}}, \eta)$, where $\eta = \|\nabla f^R\| = \|\nabla f\|$. Denoting $f^S(p) = f^R(S^{-1}(p))$, we get $[\nabla f^S]^T = S^{-T} [\nabla f^R]^T = [0, 0, 1]^T$.

Finally we rotate the surface in the xy -plane in order to align the principal curvature direction of the transformed surface $\{f^S(p) = 0\}$ with the x -axis and y -axis. This is equivalent to diagonalize the tangent part of the Hessian matrix of f^S : $\begin{bmatrix} f_{xx}^S & f_{xy}^S \\ f_{xy}^S & f_{yy}^S \end{bmatrix}$. The rotation R_2 is then a rotation of angle $\theta = \frac{1}{2} \arctan\left(\frac{-2f_{xy}^S}{f_{xx}^S - f_{yy}^S}\right)$ in the xy -plane. This leads to the function of the proposition $\tilde{f}(p) = f^S(R_2^{-1}(p)) = f(A^{-1}(p))$. Since the gradient of f^S is along the z axis, the planar rotation R_2 does not alter it. Since the Hessian matrix $H_{\tilde{f}}$ of \tilde{f} is given by the composition of quadratic forms: $H_{\tilde{f}} = R_2^{-T} H_{f^S} R_2^{-1} = R_2 H_{f^S} R_2^T$, we get $\tilde{f}_{xy} = 0$. ■

Observation In terms of degrees of freedom, the transformation A is a 3×3 matrix. From those 9 coefficients, the equiaffine restriction imposes $\det A = 1$, which reduces the degrees of freedom by one. The rotation R_1 and the scaling S each reduce the degrees of freedom by three: the angle or the scale factor, and an axis. The planar rotation R_2 has one degree of freedom: its angle. Although there is still one spare degree of freedom for the coefficients, the second derivative has a quadratic dependency on the coefficients of A , and there is no guarantee that further simplification would be feasible without deciding the sign of the metric (or equivalently the signal of the Euclidean Gaussian curvature).

(b) Simplified formulae

In this subsection, we will consider an implicit surface $\{p \in \mathbb{R}^3, f(p) = 0\}$ around point p such that $\nabla f(p) = [0, 0, 1]$ and $f_{xy}(p) = 0$. From the previous proposition, we ensure this condition for any regular point through an equiaffine map A . With this condition, we derive the simplified formulae for the implicit structures:

Tangent Since $f_x = f_y = 0$, we deduce from Equation (1):

$$\mathcal{G}_x = [1, 0, 0] \quad \text{and} \quad \mathcal{G}_y = [0, 1, 0].$$

Metric The metric reduces to a very simple expression: $d = f_{xx}f_{yy}$.

Co-normal From the metric and gradient, we deduce: $\nu = |f_{xx}f_{yy}|^{-1/4} [0, 0, 1]$.

Normal The affine normal reduces to:

$$\xi = \frac{1}{4 |f_{xx}f_{yy}|^{7/4}} \begin{bmatrix} f_{yy}^2 f_{xxx} + f_{xx} f_{yy} f_{xyy} - 4f_{xx} f_{yy}^2 f_{xz} \\ f_{xyy} f_{xxx} f_{yy} - 4f_{xx}^2 f_{yy} f_{yz} + f_{xx}^2 f_{yyy} \\ 4f_{xx}^2 f_{yy}^2 \end{bmatrix}.$$

Curvatures The curvature expressions also greatly simplify:

$$b_{11} = \frac{1}{16 f_{xx}^{11/4} f_{yy}^{7/4}} \left(8f_{xx}^2 f_{yy}^2 f_{xz}^2 - 8f_{xx}^3 f_{yy}^2 f_{zz} + 8f_{xx}^3 f_{yy} f_{yz}^2 - 4f_{xx}^2 f_{yy} f_{xxyy} - 4f_{xx} f_{yy}^2 f_{xxx} \right. \\ \left. + 7f_{yy}^2 f_{xxx}^2 + 3f_{xx}^2 f_{yy}^2 + 12f_{xx} f_{yy} f_{xxy}^2 + 2f_{xx} f_{yy} f_{xxx} f_{xyy} + 4f_{xx}^2 f_{xxy} f_{yyy} \right. \\ \left. + 24f_{xx}^2 f_{yy}^2 f_{xxz} - 24f_{xx} f_{yy}^2 f_{xz} f_{xxx} - 24f_{xx}^2 f_{yy} f_{yz} f_{xxy} \right),$$

$$b_{21} = \frac{1}{16 f_{xx}^{11/4} f_{yy}^{7/4}} \left(15f_{xx} f_{yy} f_{xxy} f_{xyy} - f_{xx} f_{yy} f_{xxx} f_{yyy} - 4f_{xx}^2 f_{yy} f_{xyyy} - 24f_{xx}^2 f_{yy} f_{yz} f_{xxy} \right. \\ \left. - 4f_{xx} f_{yy}^2 f_{xxx} + 24f_{xx}^2 f_{yy}^2 f_{xyz} - 24f_{xx} f_{yy}^2 f_{xz} f_{xxy} + 7f_{yy}^2 f_{xxx} f_{xxy} + 7f_{xx}^2 f_{xyy} f_{yyy} \right).$$

The formulae for b_{12} and b_{22} are obtained by exchanging x and y in b_{21} and b_{11} .

(c) From the geometric reduction to the general case

The previous reduction is the key to increase the numerical stability and improve the invariance of the estimated affine structures. Starting from the original implicit function f at a regular point p , we compute the transformation A , which is defined from the first and second derivatives of f at p following Proposition 1, leading to a new implicit function $\tilde{f}(\tilde{p}) = f(A^{-1}(\tilde{p}))$ with $\tilde{p} = A(p)$.

We first compute the derivatives of \tilde{f} from the derivatives of f using the chain rule:

$$\begin{aligned} \nabla \tilde{f}(\tilde{p}) &= \nabla f(p) \cdot A^{-1} \\ H_{\tilde{f}}(\tilde{p}) &= A^{-T} \cdot H_f(p) \cdot A^{-1} \\ \forall (i, j, k) \in \{x, y, z\}^3, \quad \tilde{f}_{ijk}(\tilde{p}) &= \sum_{(a,b,c) \in \{x,y,z\}^3} f_{abc}(p) A_{a,i}^{-1} A_{b,j}^{-1} A_{c,k}^{-1} \\ \forall (i, j, k, l) \in \{x, y, z\}^4, \quad \tilde{f}_{ijkl}(\tilde{p}) &= \sum_{(a,b,c,d) \in \{x,y,z\}^4} f_{abcd}(p) A_{a,i}^{-1} A_{b,j}^{-1} A_{c,k}^{-1} A_{d,l}^{-1}, \end{aligned} \tag{4}$$

where $A_{a,i}^{-1}$ is the coefficient of the inverse matrix A^{-1} of row a and column i .

From those derivatives, we use the simplified formula to compute the affine structure $\tilde{\nu}(\tilde{p})$, $\tilde{\xi}(\tilde{p})$, $\tilde{\mathcal{K}}(\tilde{p})$ and $\tilde{\mathcal{H}}(\tilde{p})$ of the implicit surface defined by \tilde{f} .

From the invariance of those structures, we deduce the affine structure of the original implicit surface $\{p \in \mathbb{R}^3, f(p) = 0\}$ at point p :

$$\begin{aligned} \tilde{\nu}(\tilde{p}) &= \nu(p) \cdot A^{-1}, \\ \tilde{\xi}(\tilde{p}) &= \xi(p) \cdot A^T, \\ \tilde{\mathcal{K}}(\tilde{p}) &= \mathcal{K}(p), \\ \tilde{\mathcal{H}}(\tilde{p}) &= \mathcal{H}(p). \end{aligned}$$

	Matrices A, A^{-1}	Mapping of $\partial(f)$	Simplified formulae	Total	Non-Simplified formulae
# Operations	749	7,335	1,783	9,867	23,690

Table 1: Number of floating point operations returned by Maple for a single point using the simplified formulae with the derivative mapping versus non-simplified formulae: the simplified formulae are more concise and comprise of mostly operations to map the derivatives (Equation (4)).

(d) On numerical stability

The simplified formulae are significantly more stable than direct computation without the transformation, as seen in our experiments (see section 5). We use the Maple software to optimize both the direct and simplified formulae, aiming at reducing the number of operations. The comparison of the number of operations in the direct and simplified formulae clearly explains the stability gained by the simplification (see Table 1).

However the main tool for the derivation of the implicit formulae comes from the implicit function theorem (Equation (1)), where all the derivatives of g are obtained through a division by f_z . Therefore any numerical implementation may suffer when the gradient is almost vanishing $\|\nabla f\| < \epsilon$. In the simplified formulae, this instability only appears in transformation A (in particular in the non-uniform scaling S).

Moreover, the Berwald-Blaschke metric degenerates ($d = 0$) when the Euclidean Gaussian curvature is close to zero. In particular at inflection points, the affine curvatures should be infinite, even though they are regular. Such divergence is delicate to handle in a numerical context. A separate handling of such inflection points has been proposed for curves through a careful local resampling [6] and could be extended to surfaces in future work. This instability remains in the simplified formulae.

4 Affine structure computation for isosurfaces

From the previous sections, we compute the affine structure of an implicit surface $\{p \in \mathbb{R}^3, f(p) = 0\}$ at one of its regular point p from the derivatives of f up to the fourth order. In this section we discuss the main tools we use to apply such calculi in a simple implicit surface extractor on a regular grid: how to approximate derivatives, how to incorporate the affine structure computation into Marching Cubes [16], and how to measure the quality of the results.

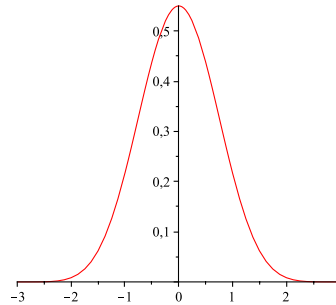


Figure 7: Spline function σ_1 of degree 5 in one variable.

(a) Discrete derivatives approximation

The formulae for the affine curvature involve all the partial derivatives of f up to the fourth order. Those 34 derivatives may be very sensitive to numerical noise on f , specially those of high order. When f is sampled on a regular grid, which is the common case for describing geometric object implicitly, a common choice to obtain such derivatives relies on discrete convolutions with splines [24]. We use in our experiments a trivariate spline function $\sigma(x, y, z)$ of degree 5 defined by $\sigma(x, y, z) = \sigma_1(x)\sigma_1(y)\sigma_1(z)$ (see Figure 7), where:

$$\sigma_1(t) = \frac{1}{60} \begin{cases} (3-t)^5 - 6(2-t)^5 + 15(1-t)^5 & , \quad 0 \leq |t| < 1 \\ (3-t)^5 - 6(2-t)^5 & , \quad 1 \leq |t| < 2 \\ (3-t)^5 & , \quad 2 \leq |t| < 3 \\ 0 & , \quad |t| > 3. \end{cases}$$

The derivatives are obtained by convolving f with the normalized derivative of the spline: $f \approx f * \sigma \Rightarrow \partial^\alpha f \approx f * (\frac{1}{c} \partial^\alpha \sigma)$. The constant c is determined for each derivation in order to compensate for the scaling from the voxel spacing to the $]-3, 3[$ domain of σ_1 and to guarantee that derivatives of monomials of degree α are correctly estimated [8].

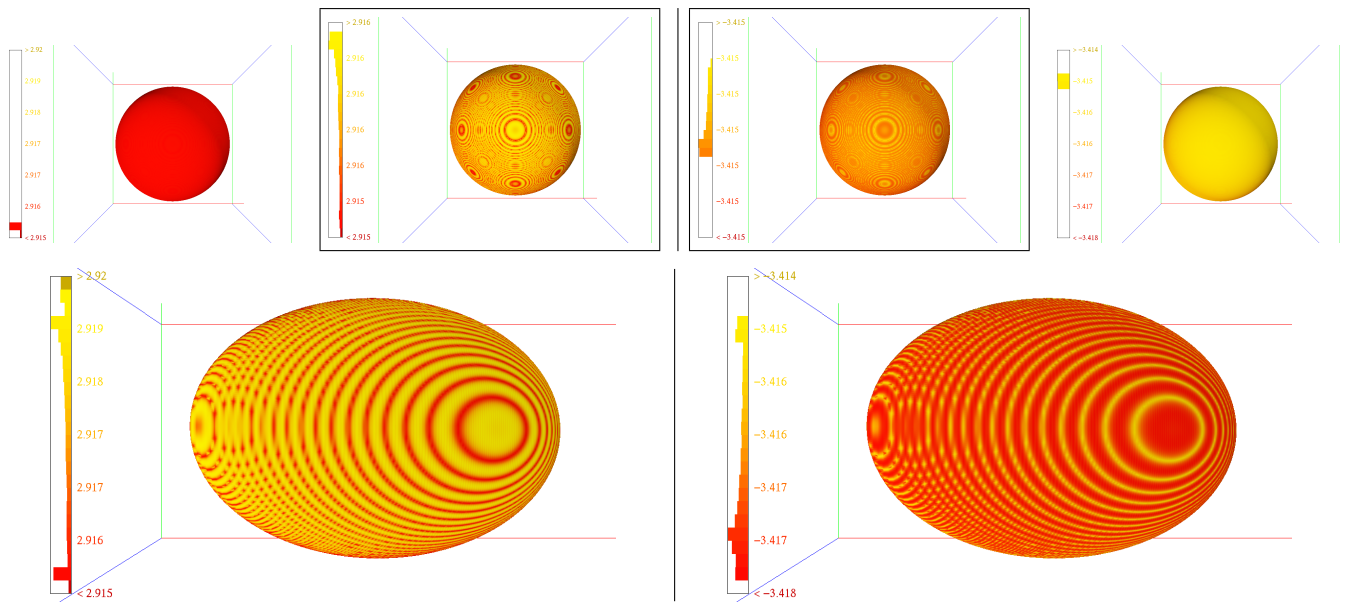


Figure 8: Incorporating the estimators inside Marching Cubes reveals the non-invariant pattern of the grid-based derivative estimation: (left) \mathcal{K} and (right) \mathcal{H} view, before (top) with a close up of the scale, and after (bottom) the affine transformation $[[0.9, 0, 0.9], [0, 2, 0], [1.1, 0, 0.6]]$.

(b) Implementation inside Marching Cubes

Marching Cubes [16] is the base algorithm for extracting implicit surfaces. It operates on each voxel of a regular grid, and eventually generate some triangles inside the voxels. The vertices of those triangles are computed by linear interpolation along the edges of the voxel, generating either 0 or 1 vertex per edge, depending if the values of the implicit function at the edge's ends have equal or different signs, respectively.

Since we can directly evaluate the derivatives through discrete convolution only at the vertices of the voxel, we can either compute the affine structure ν , ξ , \mathcal{K} and \mathcal{H} at the voxel corners (off the surface) and interpolate the structure (linearly) along the edge, or interpolate the derivatives along the edge and compute the affine structure at the Marching Cubes' vertex from those interpolated derivatives. The former option has the disadvantage of computing the affine structure off-surface, and without restriction on f , this structure may differ from the on-surface one.

Since the Marching Cubes mechanics uses linear interpolation (to avoid having more than one vertex per voxel edge), the latter option is not completely consistent: interpolating a fourth-order derivative linearly means interpolating the function itself as a polynomial of degree 4! This is visible on the sphere of Figure 8, where the very small noise variations are correlated to the grid structure. However, this last option of interpolating derivatives at the Marching Cubes' vertices and then computing the affine structure leads to better results in practice [20], as seen in the next section.

(c) Quality measures

The quality of a geometric estimator is generally measured along four criteria: invariance under geometric mapping, error compared to the exact geometric measure, convergence to the continuous measure when the sampling gets denser, and robustness to noise.

In the computation of affine structure for isosurfaces, the most delicate one is the invariance criterion since the sampling process of the implicit function f on a regular grid is not invariant under affine mapping. Moreover, when checking the invariance by comparing the affine estimators on an isosurface before and after an affine transformation, the vertices generated by the Marching Cubes algorithm are not at the corresponding positions and not uniformly distributed. Although we try to reduce this disparity in the experiments with analytic implicit function by adapting the transformed domain to a bounding box of the image of the original domain, a global invariance measure is still hard to implement. We generate some results of the next section by comparing histograms of the curvatures before and after some affine transformations, similar histograms indicating better invariance of the estimator.

5 Experiments

We experiment the two affine estimators introduced above: applying the direct formulae referred as the *direct* method and computing the local mapping A to use the simplified formulae referred as the *transformation* method. In the direct method, one of the axes has to be chosen at each point to serve as z direction in the implicit function theorem. In order to reduce the numerical instability, we choose the axis with which the gradient is most aligned, i.e. we choose x if $|f_x| > |f_y|$ and $|f_x| > |f_z|$ (see Figure 5). The transformation method follows the steps of section 3(a). We embedded those estimators in the Marching Cubes algorithm with the choices described in section 4 and use the open source of the Topological Marching Cubes [14].

Three groups of data were analyzed. First we generate analytic implicit functions (see Figures 4, 5, 8 and 2) where we compute the exact differential affine structure ν , ξ , \mathcal{K} and \mathcal{H} , in order to compute the error of our estimators (see section 2(f)). The second set of data groups other analytic implicit functions $f(p)$ (see Figures 3 and 9), where we can sample exactly the affine image of the surface through $f(A(p))$ to check for the invariance of the estimator, with the restriction discussed in section 4(c). The last kind of data are isosurfaces, read from a static regular grid, generated as distance functions to a triangulated surface (see Figures 1 and 12). Such isosurfaces are generally more complex and would be a first step to a more specific application of the affine estimators.

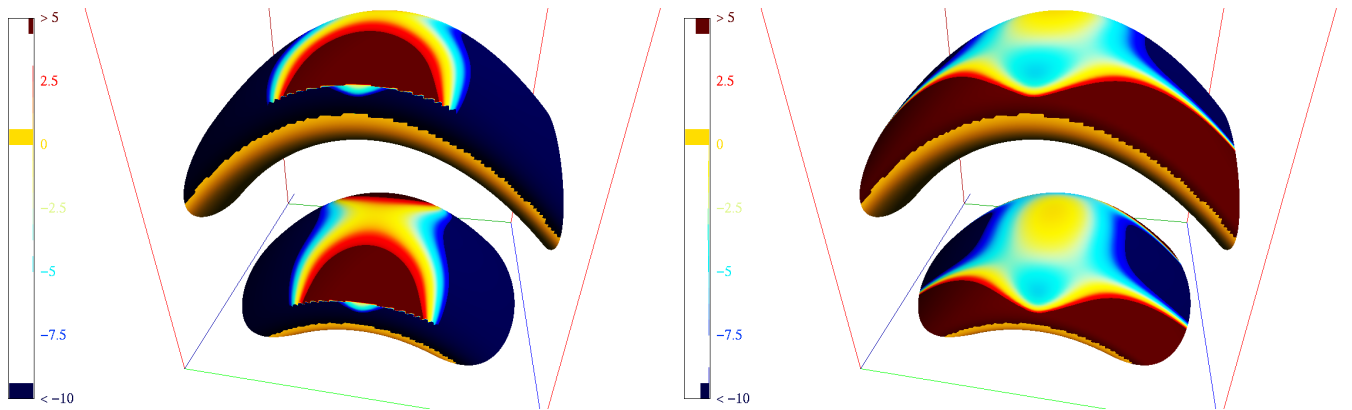


Figure 9: Sine surface of equation $2z^2 - \sin(5x + 3y^2 - 1) = 0$ in a $[-1.1, 1] \times [-1.1, 1.2] \times [-2, 2]$ box, comparing the mean curvature estimations \mathcal{H} using the direct method (left) and the transformation method (right), with the same color scales: both methods show discontinuity at the degenerated $K_e = 0$ regions, but the direct method artificially includes more discontinuities.

Numerical stability Since the definition of the affine curvature relies on a 4^{th} -order derivative, any estimator will be very sensitive to numerical error. The geometric reduction we propose allows to reduce the numerical error linked to the gradient alignment with the axis. Figure 5 clearly shows that the quality of the direct estimator decreases when the direction moves away from the axes. This is partly due to the discontinuity of the axis choice, similarly to the simpler case of Euclidean curvature of parametric curve [15], but is corrected by our reduction.

Moreover, this reduction greatly simplifies the formulae (see Table 1), which drastically improves the numerical stability. The reduction also allows to clearly identify degenerated regions where the metric d is close to 0, as in Figure 9.

Estimation error and convergence On models where we could derive the analytic expressions of the affine structure, essentially those of section 2(f), we can compute the error at each point generated by the Marching Cubes algorithm using different grid sizes. The graphics obtained are all similar to Figure 10, which is the sphere case. In the direct method the residual error and its variance do not decrease with finer grid size, while the transformation method shows converging behavior even when applying an affine transformation, i.e. looking at $f(A^{-1}p)$, while maintaining a very low error variance.

Affine Invariance As discussed in section 4(c), the measure of the affine invariance is delicate when experimenting with isosurfaces. We first generate the distribution histograms of the Gaussian affine curvature \mathcal{K} before and after an affine mapping. We compare the results obtained by the direct and transformation method on a torus model (see Figure 11). Once again the transformation method better preserves the geometric meaning of the estimated measures. On more complex isosurfaces, as the one depicted on Figures 1 and 12, the curvatures and the degenerate regions are still clearly mapped from the models of the same affine class.

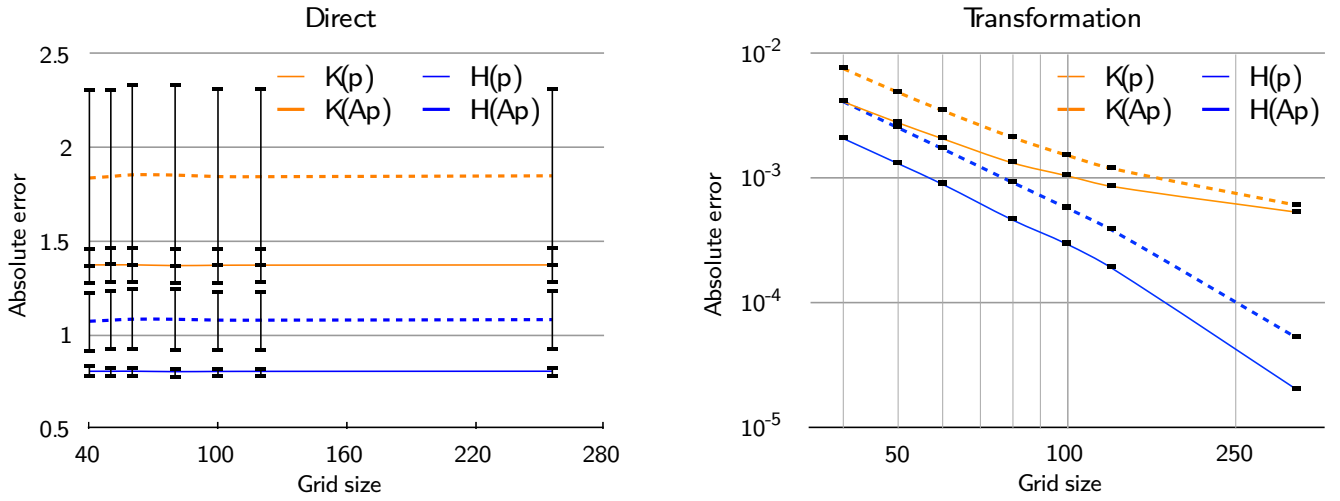


Figure 10: Convergence on the sphere model, absolute error versus grid size, before (solid) and after (dashed) the affine transformation of Figure 8, comparing the direct method (left, in linear scale) with the transformation method (right, in log/log scale) for the same sizes. The error bar represents one-fifth of the absolute error variance. For the transformation method, the relative error for \mathcal{K} starts from 0.6% for a grid size of 40 to 0.04% for a grid side of 256, and from 0.1% to 0.0007% for \mathcal{H} .

Limitations As mentioned in section 4(b), the sampling process is not affine invariant (see Figure 8). Although this introduces some error in the estimation process, it does not lead to significant loss on well sampled models as the ones of Figure 1. Moreover, as mentioned in section 3(d), the affine quantities are not well defined if the gradient ∇f of f is close to 0 or if the Euclidean Gaussian curvature K_e vanishes. While the second criterion correctly defines affine-invariant regions (see Figures 3 and 1), the first one is an intrinsic numerical problem. Finally the quality of the derivative approximations is crucial and may be improved [20], which may help in applying such estimators on noisy data.

6 Conclusion

This work proposes estimators for the local affine structure of implicit surfaces, i.e. the affine metric, co-normal and normal vectors, and affine Gaussian and mean curvatures. We introduce a geometric reduction in order to simplify the numerically intensive formulae, improving significantly the invariance of the estimators and reducing the error compared to the differential measure. We plan to extend this work by completing the affine estimators with the Pick invariant and eventually the affine signature, allowing for a complete set of estimators for differential affine invariants.

Acknowledgments

The authors would like to thank Marcos Craizer, João Paixão and Carlos Tomei for their constructive remarks and incentive. This work is partially financed by CNPq, CAPES and FAPERJ.

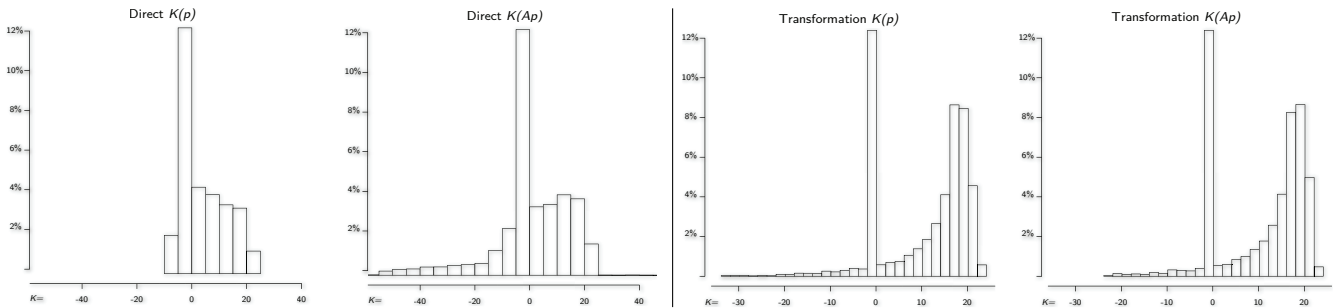


Figure 11: On the torus $z^2 - (\sqrt{x^2 + y^2} - 0.5)^2 = 0$, the distribution of the affine Gaussian curvature \mathcal{K} is better preserved under the affine transformation $[[1.4, -0.2, 0], [0.1, 0.7, 0], [0, 0, 1]]$ if using the transformation method (right) compared to the direct one (left).

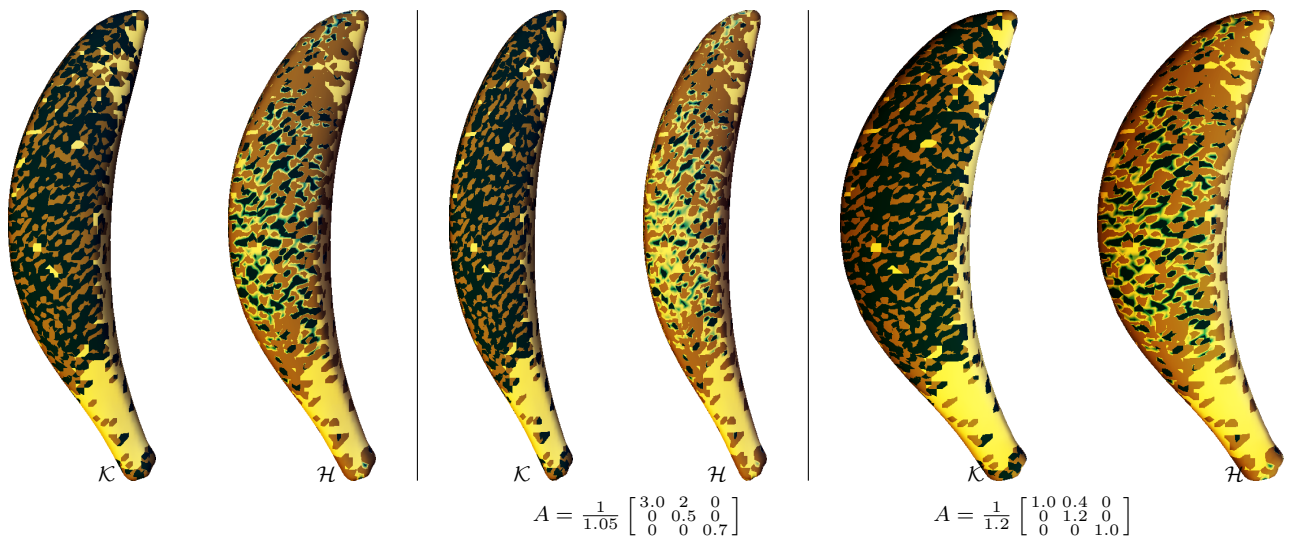


Figure 12: On a distance field to a banana on a 256^3 grid through affine transformations $p \mapsto A \cdot p$, with the affine Gaussian (\mathcal{K}) and mean (\mathcal{H}) curvatures, colored from dark to bright. Although those shapes are clearly similar, Euclidean curvatures does not match, but affine ones do.

References

- [1] K. Arbert, W. Snyder, H. Burkhardt and G. Hirzinger. Application of affine-invariant Fourier descriptors to recognition of 3-D objects. *Transactions on Pattern Analysis and Machine Intelligence*, 12(7):640–647, 1990.
- [2] S. Betelu, G. Sapiro and A. Tannenbaum. Affine invariant erosion of 3d shapes. In *International Conference on Computer Vision*, volume 2, pages 174–180. IEEE, 2002.
- [3] S. Buchin. *Affine differential geometry*. Routledge, 1983.
- [4] E. Calabi. Hypersurfaces with maximal affinely invariant area. *American Journal of Mathematics*, 104(1):91–126, 1982.
- [5] M. Do Carmo. *Differential geometry of curves and surfaces*. Prentice Hall, 1976.
- [6] M. Craizer, T. Lewiner and J. Morvan. Combining points and tangents into parabolic polygons. *Journal Math Imaging Vision*, 29:131–140, 2007.
- [7] G. Farin, J. Hoschek and M. Kim. *Handbook of computer aided geometric design*. North-Holland, 2002.
- [8] D. Forsyth and J. Ponce. *Computer vision: a modern approach*. Prentice Hall, 2002.
- [9] A. Foulonneau, P. Charbonnier and F. Heitz. Affine-invariant geometric shape priors for region-based active contours. *Transactions on Pattern Analysis and Machine Intelligence*, pages 1352–1357, 2006.
- [10] R. Gal and D. Cohen-Or. Salient geometric features for partial shape matching and similarity. *Transactions on Graphics*, 25(1):130–150, 2006.
- [11] R. Gal, A. Shamir, T. Hassner, M. Pauly and D. Cohen-Or. Surface reconstruction using local shape priors. In *Symposium on Geometry Processing*, pages 253–262. Eurographics, 2007.
- [12] R. Goldman. Curvature formulas for implicit curves and surfaces. *Computer Aided Geometric Design*, 22(7):632–658, 2005.
- [13] R. Kimmel. Affine differential signatures for gray level images of planar shapes. In *International Conference on Pattern Recognition*, page 45. IEEE, 1996.
- [14] T. Lewiner, H. Lopes, A. Vieira and G. Tavares. Efficient implementation of Marching Cubes’ cases with topological guarantees. *Journal of Graphics Tools*, 8(2):1–16, 2003.
- [15] T. Lewiner, J. Gomes, H. Lopes and M. Craizer. Curvature and torsion estimators based on parametric curve fitting. *Computers & Graphics*, 29(5):641–655, 2005.

- [16] W. Lorensen and H. Cline. Marching Cubes: A high resolution 3D surface construction algorithm. In *Siggraph*, page 169. ACM, 1987.
- [17] D. Lowe. Distinctive image features form scale invariant keypoints. *International Journal of computer Vision*, 60(2):91–110, 2004.
- [18] K. Mikolajczyk and C. Schmid. A performance evaluation of local descriptors. *Transactions on Pattern Analysis and Machine Intelligence*, 27(7):1615–1630, 2005.
- [19] K. Mikolajczyk and C. Schmid. A comparison of affine region detectors. *International Journal of Computer Vision*, 65(1):43–72, 2006.
- [20] T. Möller, R. Machiraju, K. Mueller and R. Yagel. A comparison of normal estimation schemes. In *Visualization*, pages 19–26. IEEE, 1997.
- [21] M. Mortara and G. Patané. Affine-invariant skeleton of 3d shapes. In *Shape Modeling International*, page 245. IEEE, 2002.
- [22] T. Newman and H. Yi. A survey of the marching cubes algorithm. *Computers & Graphics*, 30(5):854–879, 2006.
- [23] K. Nomizu and T. Sasaki. *Affine differential geometry: geometry of affine immersions*. Cambridge University Press, 1994.
- [24] G. Nürnberger, J. Schmidt and G. Walz. *Multivariate approximation and splines*. Birkhauser, 1997.
- [25] D. Raviv, A. M. Bronstein, M. M. Bronstein, R. Kimmel and N. Sochen. Affine-invariant geodesic geometry of deformable 3d shapes. *Computers & Graphics*, 35(3):692–697, 2011.
- [26] M. Reuter, F. Wolter and N. Peinecke. Laplace-Beltrami spectra as shape-DNA of surfaces and solids. *Computer-Aided Design*, 38(4):342–366, 2006.
- [27] F. Rothganger, S. Lazebnik, C. Schmid and J. Ponce. 3d object modeling and recognition using local affine-invariant image descriptors and multi-view spatial constraints. *International Journal of Computer Vision*, 66(3):231–259, 2006.
- [28] G. Sapiro and A. Tannenbaum. Affine invariant scale-space. *International Journal of Computer Vision*, 11(1):25–44, 1993.
- [29] M. Zuliani, L. Bertelli, C. Kenney, S. Chandrasekaran and B. Manjunath. Drums, curve descriptors and affine invariant region matching. *International Journal of computer Vision*, 26:347–360, 2008.